A new pipeline to automatically segment and semi-automatically measure bone length on 3D models obtained by Computed Tomography.

Santiago Beltran Diaz[1], Xinli Qu[1], Sarah Fung[2], Michael de Veer[3], Olga Panagiotopoulou[2] and Alberto Rosello-Diez[1].

[1]*Australian Regenerative Medicine Institute. Monash University. 3800 Clayton VIC. Australia.*

[2] *Monash Biomedicine Discovery Institute, Department of Anatomy and Developmental Biology. Monash University. 3800 Clayton VIC. Australia.*

[3]*Monash Biomedical Imaging. Monash University. 3800 Clayton VIC. Australia.*

Summary statement: Beltran Diaz et al. present a semi-automated pipeline for fast and versatile characterization of bone length from micro-CT images of mouse developmental samples.

Abstract: The characterization of developmental phenotypes often relies on the accurate linear measurement of structures that are small and require laborious preparation. This is tedious and prone to errors, especially when repeated for the multiple replicates that are required for statistical analysis, or when multiple distinct structures have to be analysed. To address this issue, we have developed a pipeline for characterization of long-bone length using micro-CT scans. It involves a semi-automated algorithm that uses the Mimics Innovation Suite package (Materialise) for automatic thresholding and fast interactive isolation and 3D-model generation of the main limb bones. All the image-processing steps are included in a user-friendly Python script. We show that the appropriate combination of scanning and *in silico* analysis conditions yields fast and reproducible length results, highly correlated with the measurements obtained via *ex vivo* skeletal preparations. Moreover, since micro-CT is not destructive, the samples can be used afterwards for histology or other applications. Our new pipeline will help developmental biologists and evolution researchers to achieve fast, reproducible and non-destructive length measurement of bone samples from multiple animal species.

INTRODUCTION

Bone-length measurement is the pillar of many research applications, such as developmental studies on limb patterning (Galloway et al., 2009; Summerbell, 1977) and growth (Marchini and Rolian, 2018; Rosello-Diez et al., 2017), evolutionary studies (Kherdjemil et al., 2016; Sears et al., 2006; Sheth et al., 2012), disease modelling (Chen et al., 1999; Li et al., 1999; Rowe et al., 2018), adult phenotyping of mutant models (Boskey et al., 2003), etc. Whereas clinical musculoskeletal research often uses non-destructive imaging as routine (Cheng and Wang, 2018), fundamental evolutionary and development (evo-devo) studies often rely on differential staining of bone and cartilage (the so-called *ex vivo* skeletal preparations) (Mead, 2020; Rigueur and Lyons, 2014) and subsequent two-dimensional (2D) imaging for quantitative comparisons of the models of interest. Despite being broadly used, the skeletal preparation technique is ridden by several disadvantages. First, it is a destructive technique in the sense that the samples cannot be used for further histological or molecular applications. Second, it involves lengthy staining and clearing of cadavers, followed by laborious and damage-prone dissection of the individual bones of interest, in order to prepare them for imaging. Third, accurate measurements depend heavily on the imaged sample being positioned as flat as possible; otherwise the apparent length will be shorter than the real one due to parallax error. As a result, measurements are often prone to user error and require multiple measurements to calculate standard error. These limitations prompted us to seek alternative methods to measure bone length in a fast and reliable way, without destroying the sample.

Micro-computed tomography (µCT) is a non-destructive imaging modality that uses multiple X-rays and computed algorithms to generate a three-dimensional (3D) image of a physical object based on the absorbance of X-ray energy (Christiansen, 2016; du Plessis et al., 2017). We reasoned that since µCT can be used to image undissected samples, it would allow us to scan multiple samples relatively fast, with the advantages of preserving their integrity in case they are needed for further processing. Moreover, computer-based image processing would in principle allow us to maximize the automation of the subsequent 3D reconstruction and measurements. In summary, our main goal was to develop a pipeline to scan multiple whole-animal samples in a batch, and bulk-process the scans with minimal user intervention, to extract linear measurements of the bones of interest. Within this general goal, we established three aims: 1) to identify standard conditions (i.e. combination of scan resolution and analysis parameters) that yield low inter-batch variability; 2) to obtain a versatile pipeline that could be applied with minimal variation to a range of developmental stages; 3) to achieve enough precision to be able to detect even small phenotypes, such as the 5-10% bone-length differences we have previously described with some of our models (Rosello-Diez et al., 2018; Rosello-Diez et al., 2017).

In µCT, the ability to independently analyse distinct tissues relies on their accurate separation through so-called segmentation (Bouxsein et al., 2010; Weissheimer et al., 2012). Since bone is a high-density tissue, it presents with high intensity in CT scans and can be readily segmented through threshold-based methods where grayscale values determine what is bone and what is background (Campbell and Sophocleous, 2014). There are several modalities of segmentation. Manual segmentation involves the

manual selection of the areas of interest section by section, and is therefore quite laborious and subjective, thus prone to user error (Rathnayaka et al., 2011). Semi-automated methods, on the other hand, use algorithms like edge detection (Rathnayaka et al., 2011) and/or local differences in grey values (Zhang et al., 2010) with some user input for initial parameters. Another common method is automated segmentation, whereby image-processing algorithms are used to segment elements of interest with minimal to no-user interaction (Heidrich et al., 2013; Okada et al., 2008; Šajn et al., 2007; Yiannakas et al., 2016). Algorithm-based automatic segmentation, however, requires the user to have programming knowledge and a thorough understanding of mathematical algorithms related to the image processing software being utilised (Rathnayaka et al., 2011).

There are a wide range of software solutions that can analyse CT data in the form of digital imaging communications in medicine (DICOM) files to segment a variety of high-contrast tissues like lungs (Reynisson et al., 2015; Weissheimer et al., 2012), liver (Huhdanpaa et al., 2011; Okada et al., 2008) and bone (Mehadji et al., 2019; Rios et al., 2014; Taghizadeh et al., 2019). After some pilot testing of both open-source and commercial solutions, we settled on the Mimics Innovation Suite (Materialise, Leuven, Belgium) as the one that most readily suited our needs. Mimics has been previously benchmarked against other programs like Syngo (An et al., 2017), OsiriX (Reynisson et al., 2015) and ITK-snap (Weissheimer et al., 2012), and some of its key features are its flexibility, ease of use, sensitive and controlled segmentations (Reynisson et al., 2015; Weissheimer et al., 2012) and the possibility to integrate Python scripting modules to further extend its automation capabilities.

Here we present a semi-automated analysis pipeline for the fast and robust characterisation of long-bone length, using Python scripting and segmentation tools of the commercially available software package Mimics, which can be used by non-experts.

RESULTS

Developing a script for bone-length measurement on µCT scans with minimal user input

A Python script was written that utilises Mimics capabilities to segment and measure the mouse bones of interest (humerus, radius, ulna, tibia and sometimes clavicle) from CT scans. This script is called BASILISC (Bone Automated Segmentation and Interactive Length Interrogation on Standardized CT scans). BASILISC is available in Github (www.github/rosellodiez/Basilisc), and designed to run in the Materialise Mimics Research software v.18 to 21, and hence there are attributes that are specific to this program. The script can be divided into 4 main sections: thresholding, landmarking, 3D modelling, measurement & export (Fig. 1A). See Supplementary Video 1 for an overview of the whole procedure.

The first Python command in BASILISC segments all the skeletal elements, using a global threshold for bone tissue (Fig. 1B). To increase its applicability to different developmental stages and scanning conditions, BASILISC was designed in such a way that the user can select among three pre-defined thresholds (Low, Medium, High) via a pop-up menu. These pre-defined values can be easily changed within the script (see Methods). The next section of the script is landmarking, which uses Mimics tools to segment

and uniquely label all bones of interest via a pop-up menu (Fig. 1C). The user is prompted to select a region (landmark) of the indicated element by simply clicking on it on one of the 2D views of the sample. BASILISC will automatically label and segment the selected element without further user interaction. In the third section of the script, once all bones of interest have been segmented and labelled accordingly, a 3D model of each skeletal element is created (Fig. 1D). Then BASILISC automatically fits a so-called centre line to each bone, running from end to end along the centre of the element. In the last section, the script automatically obtains the length of the fitted line and saves the measurement to a comma-separated text file (Fig. 1E). Once this basic method was developed, we set out to bench-mark it.

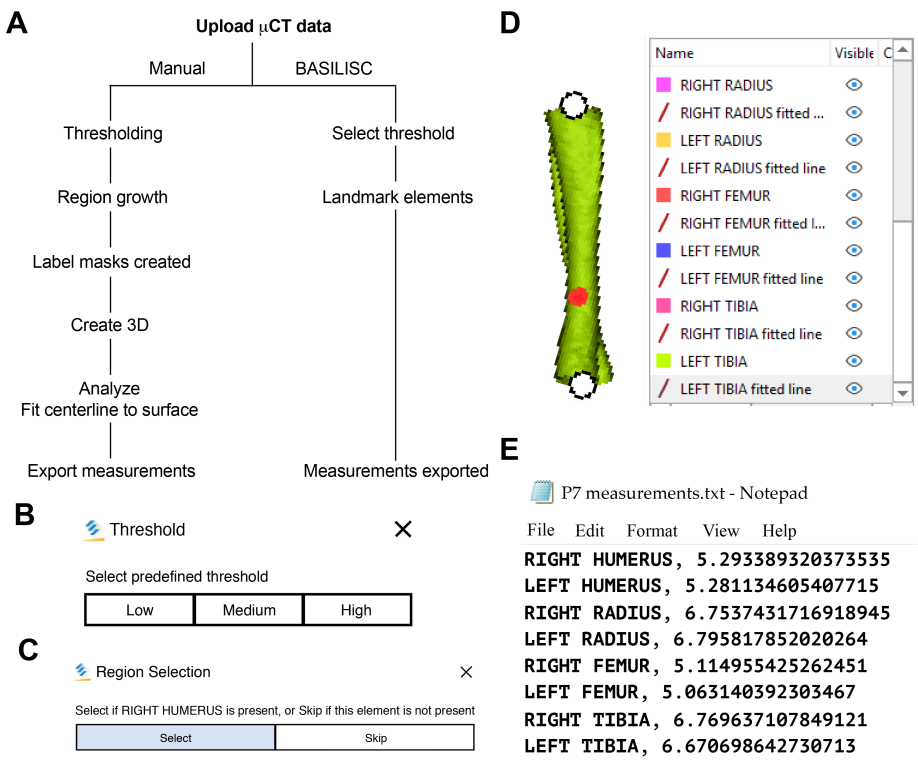

Figure 1. Bone Automated Segmentation and Interactive Length Interrogation of Standardized CT scans. A) Diagram depicting the procedure followed by the script. B-E) Representative screenshots of key steps in the process: threshold pre-selection and segmentation (B), element seeding (C), centre-line fitting (D), table export (E).

Standardized conditions to achieve robustness to batch effect at multiple stages

A semi-automatic protocol to measure bone length would only be useful if it yielded consistent measurements for a given sample, scanned and analysed repeatedly on different days. We thus explored different scan resolutions and imaging thresholds to analyse technical replicates from two different postnatal day (P) 7 mouse specimens (see Methods), and assessed the reproducibility of the results. 40-μm scans showed relatively high inter-batch effect, especially for hindlimb bones, regardless of the threshold (Fig. 2A, B), whereas 20-μm scans yielded more consistent measurements, including hindlimb bones, especially for the lower threshold (Fig. 2C, D). To compare the batch effect more quantitatively, we then calculated the

coefficient of variability (CV) for each bone's measurements across the three batches, and compared the CV for the different conditions and bones. A 2-way analysis of variance (ANOVA) showed that there was a significant effect of the imaging & analysis conditions, although the extent of it was likely distinct for the different bones (Fig. 2E). In summary, these results identified a 20-µm resolution and a 398-Hounsfeld units (HU) threshold as the optimal conditions to minimize inter-batch variability in this type of samples (i.e. P7 mouse long bones).

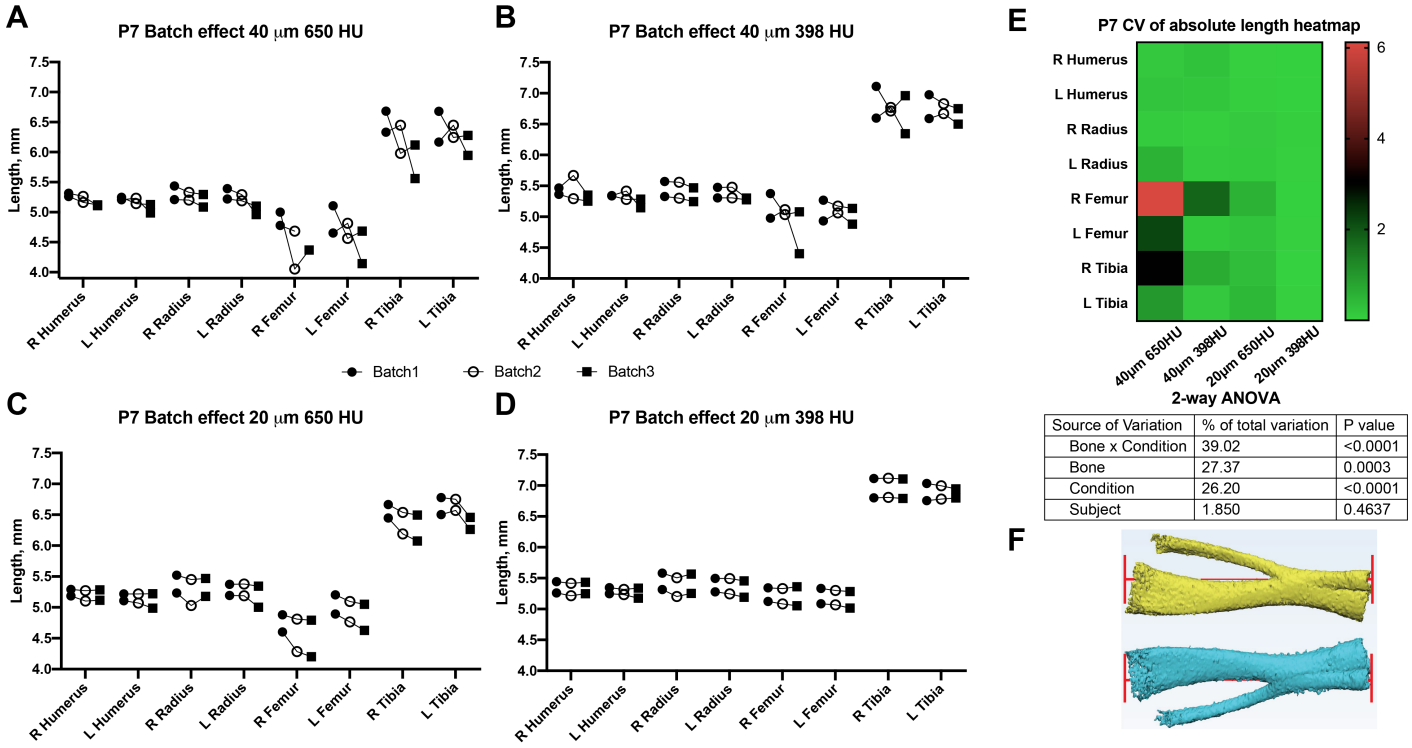

Source of Variation	% of total variation	P value
Bone x Condition	39.02	<0.0001
Bone	27.37	0.0003
Condition	26.20	<0.0001
Subject	1.850	0.4637

Figure 2. Assessment of batch effect for multiple P7 bones across different scan and analysis conditions. A-D) Measured length for the indicated bones of two P7 mouse pups, each scanned in triplicate (on three different days) at either 40 (A, B) or 20-µm resolution (C, D), and analysed with either a 650-HU (A, C) or a 398-HU threshold (B, D). L, R: left, right. E) Top: Heatmap for the Coefficient of Variability (CV, %) between the three batches of the indicated measurements. Bottom: 2-way ANOVA table showing the contribution and associated p-value of each source of variation of the experiment. F) Representative examples of the generated tibial 3D models (left and right from the same specimen) and their fitted centrelines.

Next, in order to test the versatility of BASILISC across developmental stages, we performed a similar batch-effect analysis at embryonic day (E) 17.5. Similar to the P7 experiment, we performed a battery of scan & measurement analyses exploring different resolution and threshold values (see Methods). At this stage, most of the conditions performed similarly in terms of reproducibility across batches, except for low resolution and low threshold, for which some femora were not properly segmented and as a consequence their length was overestimated (Fig. 3A-D). Although there was no overall difference in the CV across conditions (Fig. 3E), the data trends suggested that a 398-HU threshold outperformed a 226-HU threshold and length variation due to differences in scan resolution were minimised with a 398-HU threshold.

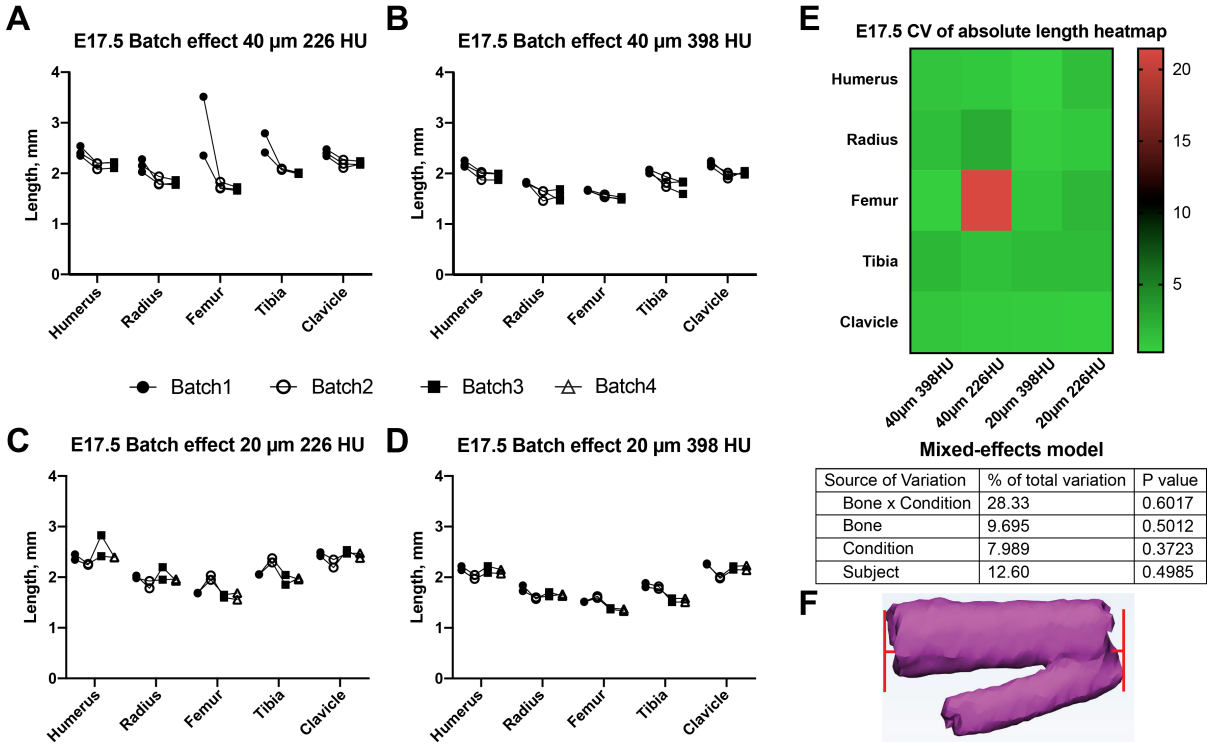

Mixed-effects model

Source of Variation	% of total variation	P value
Bone x Condition	28.33	0.6017
Bone	9.695	0.5012
Condition	7.989	0.3723
Subject	12.60	0.4985

Figure 3. Assessment of batch effect for multiple E17.5 bones across different scan and analysis conditions. A-D) Measured length for the indicated bones of two or three E17.5 mouse foetuses, each scanned in triplicate (or quadruplicate) at either 40 (A, B) or 20-µm resolution (C, D), and analysed with either a 226-HU (A, C) or a 398-HU threshold (B, D). E) Top: Heatmap for the Coefficient of Variability (CV, %) between the batches of the indicated measurements. Bottom: mixed-effects model table showing the contribution and associated p-value of each source of variation of the experiment. F) Representative example of the generated tibial 3D models and its fitted centreline.

Internal consistency across different stages, scan resolutions and segmentation thresholds

One of the advantages of working with paired bones is the possibility of assessing internal consistency of the BASILISC method by measuring the left/right ratio for each bone and condition. We therefore calculated a left/right ratio for the P7 samples, including replicates, to determine how close the ratio was to the hypothetical value of 1 (i.e. equally long left and right paired bones) and how much variability there was between replicates. As shown in Fig. 4A, 20-µm scan resolution and a threshold at 398 HU again had the lowest inter-batch variability and the L/R ratio was remarkably close to 1. As parameters moved from these optimal settings, there were several bones (typically femur, tibia and sometimes radius) for which either the average value was not as close to 1 as for other bones, and/or the variability between batches was higher than 5% (Fig. 4A). Similarly, we calculated internal ratios for E17.5 bones to determine optimal scan and segmentation parameters. In this case we chose the ratio of each bone's length over the clavicle bone length, as a normalisation approach that could be achievable in the case that contralateral bones were not available (as it was our case for these scavenged samples). This ratio obviously varies from bone to bone, but the variability of each measurement across replicates is in this case the parameter of interest to estimate the precision of the approach. As shown in Fig. 4B, with a threshold of 226 HU, some bones showed high inter-batch variability (and even artefacts in the 3D model, not shown), regardless of the

resolution. On the other hand, at 398 HU the 3D models were faithful and the variability quite reduced, especially at 40 µm.

In summary, these results suggest that a 398-HU threshold works well across a range of stages (E17.5 to P7). Whereas the optimal resolution seemed to be more stage-specific, we concluded that 20 µm is a good compromise value for the range of stages we analysed.

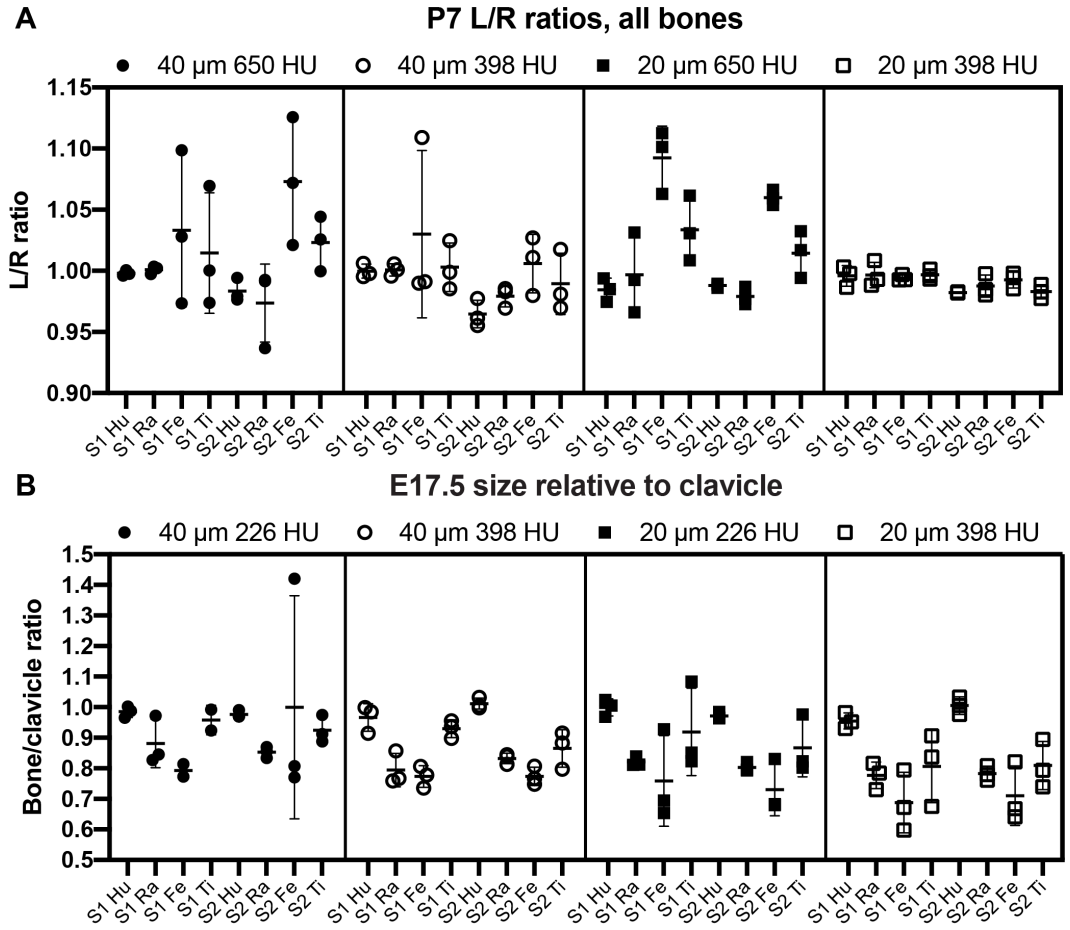

Figure 4. The comparison of intra-specimen ratios reveals the most reproducible conditions for scan and analysis. A) Left/right ratio of bone length (mean±SD) for the indicated bones and conditions at P7. Hu/Ra/Fe/Ti, Humerus/Radius/Femur/Tibia. S1-S2, specimens 1 and 2. B) Similar to A), except the ratio of length of the indicated bones to the length of the clavicle is shown for scans of E17.5 embryos.

Comparison of bone lengths obtained via BASILISC and skeletal preparations on the same samples

We next compared the bone lengths obtained by BASILISC with the lengths obtained from the same samples via skeletal preparations and digital measurement, a method frequently-used in developmental biology studies. We used eight long bones from three different specimens at P7. The linear relationship between both measurements was very good in all conditions (Fig. 5, p-value for Pearson correlation <0.0001 in all cases), and the slopes were not significantly different (p=0.3298), with an average common value of 0.9642. As expected, however, the BASILISC measurements that used lower thresholds tended to overestimate bone length (as the resulting 3D model includes less dense tissue), as indicated by the differences in the intercepts with the axes (Fig. 5, p<0.0001). Overall, the conditions that yielded measurements more reliably correlated to the skeletal preparations were 20-µm resolution and 398-HU

threshold.

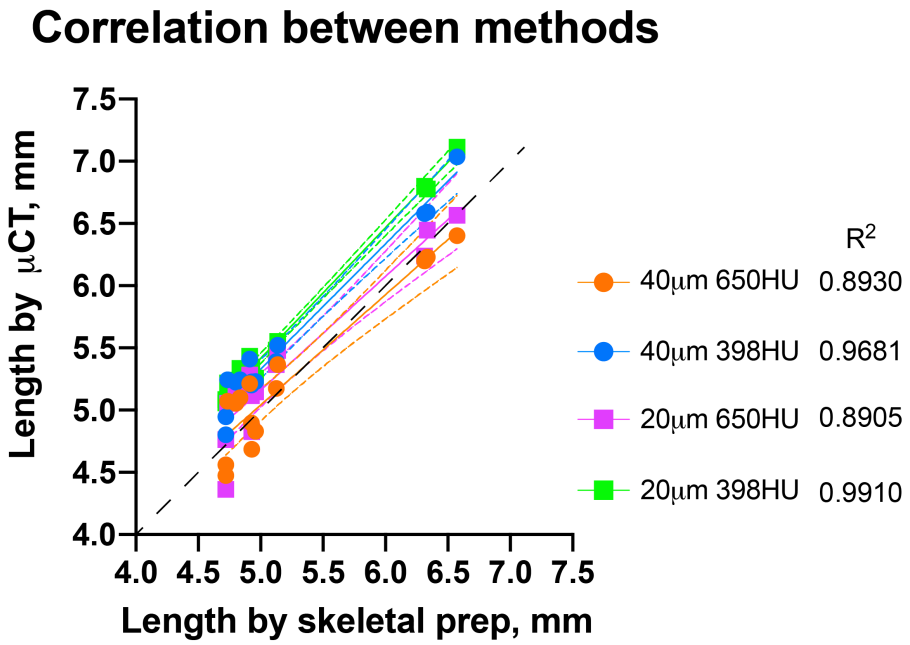

40μm 650HU	40μm 398HU	20μm 650HU	20μm 398HU
Y = 0.8863*X + 0.6085	Y = 1.007*X + 0.2938	Y = 0.9144*X + 0.5874	Y = 1.049*X + 0.1692

Figure 5. Correlation between BASILISC and the measurements obtained via classic skeletal preparations. The graph shows the bone length measurements obtained via skeletal preparations (prep.) (X axis) and BASILISC (Y axis), for four different combinations of imaging resolution and segmentation threshold (averages of 2-3 technical replicates are shown). The dashed black line represents a 1:1 correlation, for reference. Solid coloured lines represent the regression line for each combination, and the dashed ones are the 95% confidence interval of the regression. The coefficient of determination (R^2) is indicated next to the graph legend. The table shows the slope and Y-intercept for each of the BASILISC conditions used.

DISCUSSION

Here we have presented a fast and easy method to determine calcified bone length from μCT scans of whole mouse samples, without the need for dissecting the limbs, skinning or eviscerating the bodies. We tested our algorithm on a range of developmental stages (E17.5 through P7) that covers 9 days of very fast growth (Sanger et al., 2011).

Advantages over classic skeletal preparations

As any developmental biologist working on limb patterning and/or growth has experienced, analysing one litter's worth of samples by the classic method of skeletal preparation, limb microdissection, photograph acquisition and length measurement on the 2D pictures takes at least ten days and close to twenty hours of dedicated hands-on work (Rigueur and Lyons, 2014). With the BASILISC approach, decapitation and fixation of the mouse bodies takes just a few minutes per litter; scan time is roughly ten minutes per sample (plus thirty minutes of set up per imaging session); data loading and analysis takes ~5 minutes per scan. On average, this amounts to three-four hours of hands-on work per litter. Another advantage is that the measurement is three-dimensional, as opposed to two-dimensional, and therefore impervious to orientation

errors. Lastly, the scan is not destructive, and therefore the samples can be later on processed for histology or other procedures (Baier et al., 2019; Hopkins et al., 2015).

Comparison to previous automation approaches

In principle, the ideal pipeline for the kind of analysis that we perform here would be a fully automated method that recognised each of the long bones from a full-body scan, measured their length and exported those measurements without user intervention. In fact, there have been very impressive attempts at achieving this goal, combining object-based image analysis (that utilises shape and context-dependent information in addition to pixel intensity values) with machine learning. For example, Heidrich et al. (Heidrich et al., 2013) used Cognition Network Technology to extract objects and their properties from µCT data of chicken embryos at multiple stages, and then used these data to train a machine learning tool for automatic long bone classification. BASILISC is obviously far from achieving that level of automation, and implementing machine learning would probably require working with another software package. However, one of the strengths of BASILISC stems from its simplicity, as it can be used directly on any set of data, with minimal modification of the script. Contrary to this simplicity, the pipeline described in (Heidrich et al., 2013) required a large training set of close to 3,000 instances, and also complex iterative thresholding methods. Moreover, although the classification achieved via this complex process was remarkably accurate, it still required supervision and was only applied to a reduced developmental window.

In contrast to other automation procedures where edge detection has been used to determine optimal thresholds (Rathnayaka et al., 2011; Zhang et al., 2010), here we rely on a global threshold optimized by trial and error to find an optimal range of grey values. BASILISC could be further refined by implementation of widely used edge detection algorithms to further improve the segmentation process and potentially increase the accuracy of the measurements obtained. However, since intensity can vary across the length of long bones (Rathnayaka et al., 2011), edge detection would require the use of multiple thresholds to reduce the degree of error in segmentation. Thus, here we opt for a single global threshold to extend the capabilities of the algorithm for a range of developmental stages.

To our knowledge this is the first algorithm that makes use of the Python library within the Mimics software to automate the segmentation, 3D modelling and analysis of length of skeletal elements. Previously, Mimics has been complemented with other scripting languages like MATLAB (Huhdanpaa et al., 2011) for image processing before segmenting the data, or software like Creo elements (Rios et al., 2014) to analyse scans after they have been segmented. In the latter case, though, the reference points for length measurement had to be manually selected, which is a time-consuming step to do in 3D. Through BASILISC, segmentation and length measurements can all be obtained within the one program and extensive programming knowledge is not required. Furthermore, we provide a processing pipeline that extends from optimized scanning conditions of mouse samples across a range of developmental stages, to streamlined image processing and data analysis, making BASILISC a readily available tool for the research community. Of course, for BASILISC to have widespread use, it would need to be applied to open-source software.

While this is in principle possible, said software would need to fulfil two requirements: utilise Python scripts, and have similar segmentation and masking tools as Mimics. We are currently exploring a few promising open-source options.

Comparison with 'real' length measurements

Strictly speaking, the 'true value' of bone length cannot be obtained with absolute certainty by any method, as no measurement is devoid of error. For example, the classic skeletal preparation method involves quite a harsh procedure, including increasing gradients of glycerol that can shrink the sample up to 3-6% (Mabee et al., 1998). However, given the widespread use of skeletal preparation, flat mounting and imaging to obtain 2D length estimations, we compared the measurements obtained by the BASILISC approach with the length obtained by skeletal preparations (Rigueur and Lyons, 2014). Of note, all conditions showed remarkable correlation between both methods, with 20-µm resolution and 398-HU threshold yielding measurements very well correlated to those obtained via skeletal preparations across the whole range of lengths analysed. One important consideration is that the centreline fitting method generates the longest possible distance, which in some cases is not strictly running parallel to the element's main axis (e.g. Fig. 2F). This obviously generates a small bias in the measurement, but as long as the same method is used to compare different experimental conditions, this bias will be consistent and is not expected to contribute to the observed biological effect.

Limitations and future improvements

Some long bones are often segmented together in our pipeline, most often tibia and fibula (Fig. 2F and 3F), and for young stages radius and ulna. This is because their automatic separation would require too high a threshold. While radius and ulna can be quickly separated manually using the *Split_mask* function (see Methods), this is not feasible for the tibia and fibula, because their interaction surface is too large. This issue has some impact on the tibial measurements, because the fibula protrudes a bit farther than the tibia on the distal end (Fig. 2F and 3F). However, the effect is quite minor and we showed that under the right conditions the error is very consistent, as the left/right ratio for the tibia is quite tightly centred on 1 (Fig. 2). Therefore, the slightly overestimated tibial lengths can still be used for comparison purposes between different genotypes and/or treatments. The decision to invest more time in splitting them as opposed to accept the error is up to the user and depends on two main aspects: the degree of accuracy desired and the time investment required to correct the error in all samples. In our case, we opted not to correct this segmentation error, as the minor gain in accuracy would be outweighed by the extra time investment.

The aforementioned limitation would be corrected with an automatic classification system based on machine learning (Heidrich et al., 2013), but the implementation of these methods is still not supported in the Mimics scripting module. If this capability is implemented in the future, it could speed up image processing even further, as in theory no user intervention would be required to seed landmarks on the bones of interest.

Other applications

The current BASILISC pipeline only measures length of the elements, because it fits a centreline to the 3D models of the bones. However, it could in principle be adapted to measure width, by fitting a cylinder to the model and interrogating the width of the cylinder. This approach would require careful selection of the fitting parameters, so that the surface of the cylinder coincides with the surface of the 3D model. Along these lines, we have tentatively fitted vertebral bodies to the shapes of spheres (not shown), in order to calculate the distance between the centres of the spheres as a proxy for inter-vertebral distance. This application could be useful for developmental biologists studying axis elongation and segmentation.

SUPPLEMENTARY INFORMATION

Supplementary Video 1 caption. Overview of the BASILISC process performed on one of the scans used for this study. The messages prompted by the script were taken as screenshots and added to the video clip. Please note that an artefact of the video capture causes the mouse cursor to be shown slightly displaced from its real position.

MATERIALS AND METHODS

Animal experiments

Mouse embryo and pup samples were scavenged from other experiments in the Rosello-Diez lab, approved by the Animal Ethics Committee at Monash University (protocol 17048). Wild-type E17.5 samples were obtained from Asmu:Swiss crosses. P7 samples consisted of tTA-negative littermates (phenotypically wild-type) obtained from crosses of females containing the left-lateral plate mesoderm specific *Pitx2-Cre* (Shiratori et al., 2006) and a cartilage-specific *Col2a1-tTA* (Rosello-Diez et al., 2018) with males bearing a *Tigre*$^{Dragon\text{-}DTA}$ allele (Ahmadzadeh et al., 2020).

Micro-CT scans

A Siemens Inveon PET-SPECT-CT Small Animal scanner in CT modality was used for all experiments. Parameters: 20- and 40-µm resolution, 360 projections at 80 kV, 500 µA, 600 ms exposure with a 500ms settling time between projections. Binning was applied to vary resolution with 2x2 for 20µm and 4x4 for 40µm scans and data was reconstructed using a Feldkamp algorithm. The samples (beheaded embryo and pup bodies) were placed in supine position over custom-fitted foam bedding, so that the limbs were not in contact with any hard surface.

Mimics software and pipeline

Mimics Research (v21.0; Materialise, Leuven, Belgium) equipped with the scripting module was used to develop the analysis pipeline and the Python script described here. See Results for an overview and each step in the process is outlined in detail below.

Thresholding: As soon as the DICOM data is uploaded into Mimics, the first step is to distinguish the bones from all the other tissue by defining a range of Hounsfield Units (HU) that corresponds to bone density. The first Python command in BASILISC creates a mask labelled "ALL", which will segment all the skeletal elements present, creating a global threshold specific to this mask. Since the goal was to measure the developing mineralised part from end to end, this step had to detect immature trabecular bone at the ends of the growing elements. In our uncalibrated µCT scans, we realised that the custom minimum threshold for bone tissue defined by Mimics (226 HU) often over-represented the actual bone tissue in the scans as it selected a greater area of tissue. The optimal lower threshold for the developmental stages of interest had thus to be determined empirically. Although Mimics can take both gray scale values (GV) and HU units, the input in the script can only be into GV, and therefore the first step was to transform the data into GV to adequately segment all bones from the rest of the tissue. This is achieved through the "segment" attribute seen on the last line of code for this section. In principle, different optimal thresholds exist for different scanning conditions and certainly for different developmental stages, as the ratio between woven and lamellar bone decreases, and hence BASILISC was designed in such a way that the user can select among three pre-defined thresholds via a pop-up menu. This can be easily changed within the following section of the script (pre-defined values appear in orange font):

```
#setting threshold based on developmental stage, scanning conditions, etc.
mask_all = mimics.data.masks[0]
threshold = mimics.dialogs.question_box(message = "Select pre-defined threshold", title =
"Threshold", buttons = "Low;Medium;High")
if threshold == "Low":
    low_hu = 195
    high_hu = 2000
    l_t = mimics.segment.HU2GV(low_hu)
    h_t = mimics.segment.HU2GV(high_hu)
    mimics.segment.threshold(mask=mask_all,threshold_min=l_t,threshold_max=h_t)
elif threshold == "Medium":
    low_hu = 300
    high_hu = 3500
    l_t = mimics.segment.HU2GV(low_hu)
    h_t = mimics.segment.HU2GV(high_hu)
    mimics.segment.threshold(mask=mask_all,threshold_min=l_t,threshold_max=h_t)
else:
    low_hu = 398
    high_hu = 5000
    l_t = mimics.segment.HU2GV(low_hu)
    h_t = mimics.segment.HU2GV(high_hu)
    mimics.segment.threshold(mask=mask_all,threshold_min=l_t,threshold_max=h_t)
```

Landmarking: The purpose of this step is to segment and uniquely label all the bones of interest, using Mimics tools. This is achieved using a function that prompts the user (via a pop-up window) to select a landmark on the bone of interest. The first step in landmarking is to select the bones of interest to create a list of "landmarks". This list contains the unique name of each selected bone and defines the order of segmentation during the process. The "indicate_landmark" function guides the user through each of the bones to be segmented by means of a dialogue box, asking the user whether a given element is present in the scan or not and with two active buttons: "Select" & "Skip" (Fig. 1C). The user has the option to skip an element if a given bone is not present in the scan, this would then be excluded from the analysis. If the "Select" button is activated, a second dialogue box prompts the user to select a region (landmark) of the

indicated element by simply clicking on it on one of the 2D views of the sample. BASILISC will automatically label and segment the selected element without further user interaction, through the Mimics "region_grow" function. A FOR loop has been included in the BASILISC script when executing the "indicate_landmark" function, so that the steps above are recursively followed for each of the bones of interest sequentially, using the name of each bone as an index within the FOR loop.

Generation of 3D models: Once all the elements of interest have been segmented and labelled accordingly, a function has been created in BASILISC that creates 3D models of each element, "create_3D". A FOR loop in the script steps through each of the segmented bones and creates a 3D model of each at the highest possible resolution (Fig. 1D). This provided the most accurate measurements possible and since a limited number of bones are analysed, computing time to create each 3D model did not increase significantly.

Measurement: Once BASILISC has automatically made 3D models, it will fit a centre line to each bone within the "create_3D" function. This is achieved through the "analyze.create_line_fit_to_surface" attribute in Mimics. The script has been designed to then automatically obtain the length of the fitted line and save the measurement in a text file (Fig. 1E). Since this step is included within the function described above, which includes a FOR loop, the line is fitted as each 3D element is made, and the measurement is recorded progressively. The text file created will have the name of the given part, e.g. RIGHT HUMERUS, followed by a comma and the corresponding length of the element. This step is done automatically without any user input required after the landmarking step has been finalized. As the file created is only labelled with the name of the developmental stage created, the user should change the name of the text file to be sample specific before analysing the next sample.

Manual corrections during image analysis

For E17.5 samples, the radius and ulna are segmented together at the thresholds we use, but they could be easily separated using the *Split mask* function of Mimics, as their interaction surface was quite reduced.

Pipeline benchmarking

For Figures 2 and 3, each specimen was scanned in triplicate or quadruplicate (on three or four different days), at two resolutions each (20 and 40 µm), and each of the 6 scans was segmented at two different lower thresholds (650 and 398 HU for P7, 398 and 226 HU for E17.5) to perform length measurements. Humerus, radius, femur, tibia and clavicle (the latter only for E17.5) were analysed for two (P7) or three (E17.5) different specimens.

Skeletal preparations

After embryo collection, the skin, internal organs and adipose tissue were removed. The samples were then fixed in 95 % EtOH overnight at room temperature. To remove excess fat, the samples were then incubated in acetone overnight at room temperature. To stain the cartilage, the samples were submerged in a glass

scintillation vial containing Alcian blue solution (0.04 % (w/v), 70 % EtOH, 20 % acetic acid) and incubated at least overnight at room temperature. The samples were destained by incubating them in 95% EtOH overnight, and then equilibrated in 70% EtOH, prior to being pre-cleared in 1% KOH solution for 1-10h at room temperature (until blue skeletal elements were seen through). The KOH solution was replaced with Alizarin red solution (0.005 % (w/v) in 1% KOH) for 3–4h at room temperature. The Alizarin red solution was then replaced with 1-2% KOH until most soft tissues were cleared. For final clearing, the samples were progressively equilibrated through 20% glycerol:80% (1%KOH), then 50% glycerol:50% (1% KOH) and finally transferred to100% glycerol for long-term storage.

Acknowledgements

We thank members of the Rosello-Diez and McGlinn's labs for constructive feedback, Hyab Mehari Abraha (Panagiotopoulou lab) for Mimics training and Noramira Azlan (Materialise) for providing a Mimics trial license for the initial steps of the project. The authors acknowledge the facilities and scientific and technical assistance of the National Imaging Facility (NIF), a National Collaborative Research Infrastructure Strategy (NCRIS) capability at Monash Biomedical Imaging (MBI), a Technology Research Platform at Monash University. We acknowledge the technical assistance of Tara Sepehrizadeh who is a NIF Facility Fellow.

Competing interests

There are no competing interests.

Funding

This work was supported by grants from the Human Frontiers Science Program (CDA00021/2019) to A.R-D. and a NIF Facility Fellowship to M. dV. The Australian Regenerative Medicine Institute is supported by grants from the State Government of Victoria and the Australian Government.

References

Ahmadzadeh, E., Bayin, N. S., Qu, X., Singh, A., Madisen, L., Stephen, D., Zeng, H., Joyner, A. L. and Rosello-Diez, A. (2020). A collection of genetic mouse lines and related tools for inducible and reversible intersectional misexpression. *Development* **147**.

An, G., Hong, L., Zhou, X.-B., Yang, Q., Li, M.-Q. and Tang, X.-Y. (2017). Accuracy and efficiency of computer-aided anatomical analysis using 3D visualization software based on semi-automated and automated segmentations. *Annals of Anatomy - Anatomischer Anzeiger* **210**, 76-83.

Baier, W., Mangham, C., Warnett, J. M., Payne, M., Painter, M. and Williams, M. A. (2019). Using histology to evaluate micro-CT findings of trauma in three post-mortem samples - First steps towards method validation. *Forensic Sci Int* **297**, 27-34.

Boskey, A. L., van der Meulen, M. C. and Wright, T. M. (2003). Guidelines for describing mouse skeletal phenotype. *J Orthop Res* **21**, 1-5.

Bouxsein, M. L., Boyd, S. K., Christiansen, B. A., Guldberg, R. E., Jepsen, K. J. and Müller, R. (2010). Guidelines for assessment of bone microstructure in rodents using micro–computed tomography. *Journal of Bone and Mineral Research* **25**, 1468-1486.

Campbell, G. M. and Sophocleous, A. (2014). Quantitative analysis of bone and soft tissue by micro-computed tomography: applications to ex vivo and in vivo studies. *Bonekey Rep* **3**, 564-564.

Chen, L., Adar, R., Yang, X., Monsonego, E. O., Li, C., Hauschka, P. V., Yayon, A. and Deng, C. X. (1999). Gly369Cys mutation in mouse FGFR3 causes achondroplasia by affecting both chondrogenesis and osteogenesis. *The Journal of clinical investigation* **104**, 1517-1525.

Cheng, X. G. and Wang, Y. X. J. (2018). Orthopaedic imaging for translational research and clinical application. *J Orthop Translat* **15**, A1-A2.

Christiansen, B. A. (2016). Effect of micro-computed tomography voxel size and segmentation method on trabecular bone microstructure measures in mice. *Bone Rep* **5**, 136-140.

du Plessis, A., Broeckhoven, C., Guelpa, A. and le Roux, S. G. (2017). Laboratory x-ray micro-computed tomography: a user guideline for biological samples. *Gigascience* **6**, 1-11.

Galloway, J. L., Delgado, I., Ros, M. A. and Tabin, C. J. (2009). A reevaluation of X-irradiation-induced phocomelia and proximodistal limb patterning. *Nature* **460**, 400-404.

Heidrich, A., Schmidt, J., Zimmermann, J. and Saluz, H. P. (2013). Automated Segmentation and Object Classification of CT Images: Application to In Vivo Molecular Imaging of Avian Embryos. *Int J Biomed Imaging* **2013**, 508474-508474.

Hopkins, T. M., Heilman, A. M., Liggett, J. A., LaSance, K., Little, K. J., Hom, D. B., Minteer, D. M., Marra, K. G. and Pixley, S. K. (2015). Combining micro-computed tomography with histology to analyze biomedical implants for peripheral nerve repair. *J Neurosci Methods* **255**, 122-130.

Huhdanpaa, H., Douville, C., Baum, K., Krishnamurthy, V. N., Holcombe, S., Enchakalody, B., Wang, L., Wang, S. C. and Su, G. L. (2011). Development of a quantitative method for the diagnosis of cirrhosis. *Scand J Gastroenterol* **46**, 1468-1477.

Kherdjemil, Y., Lalonde, R. L., Sheth, R., Dumouchel, A., de Martino, G., Pineault, K. M., Wellik, D. M., Stadler, H. S., Akimenko, M. A. and Kmita, M. (2016). Evolution of Hoxa11 regulation in vertebrates is linked to the pentadactyl state. *Nature* **539**, 89-92.

Li, C., Chen, L., Iwata, T., Kitagawa, M., Fu, X. Y. and Deng, C. X. (1999). A Lys644Glu substitution in fibroblast growth factor receptor 3 (FGFR3) causes dwarfism in mice by activation of STATs and ink4 cell cycle inhibitors. *Hum Mol Genet* **8**, 35-44.

Mabee, P. M., Aldridge, E., Warren, E. and Helenurm, K. (1998). Effect of Clearing and Staining on Fish Length. *Copeia* **1998**, 346-353.

Marchini, M. and Rolian, C. (2018). Artificial selection sheds light on developmental mechanisms of limb elongation. *Evolution* **72**, 825-837.

Mead, T. J. (2020). Alizarin Red and Alcian Blue Preparations to Visualize the Skeleton. *Methods Mol Biol* **2043**, 207-212.

Mehadji, B., Ahmed, Y. and Berteau, J.-P. (2019). A novel approach for computing 3D mice distal femur properties using high-resolution micro-computed tomography scanning. *Micron* **121**, 1-7.

Okada, T., Shimada, R., Hori, M., Nakamoto, M., Chen, Y.-W., Nakamura, H. and Sato, Y. (2008). Automated Segmentation of the Liver from 3D CT Images Using Probabilistic Atlas and Multilevel Statistical Shape Model. *Academic Radiology* **15**, 1390-1403.

Rathnayaka, K., Sahama, T., Schuetz, M. A. and Schmutz, B. (2011). Effects of CT image segmentation methods on the accuracy of long bone 3D reconstructions. *Medical Engineering & Physics* **33**, 226-233.

Reynisson, P. J., Scali, M., Smistad, E., Hofstad, E. F., Leira, H. O., Lindseth, F., Nagelhus Hernes, T. A., Amundsen, T., Sorger, H. and Langø, T. (2015). Airway Segmentation and Centerline Extraction from Thoracic CT – Comparison of a New Method to State of the Art Commercialized Methods. *PLOS ONE* **10**, e0144282.

Rigueur, D. and Lyons, K. M. (2014). Whole-mount skeletal staining. *Methods Mol Biol* **1130**, 113-121.

Rios, D., Jansson, K. S., Martetschlager, F., Boykin, R. E., Millett, P. J. and Wijdicks, C. A. (2014). Normal curvature of glenoid surface can be restored when performing an inlay osteochondral allograft: an anatomic computed tomographic comparison. *Knee Surg Sports Traumatol Arthrosc* **22**, 442-447.

Rosello-Diez, A., Madisen, L., Bastide, S., Zeng, H. and Joyner, A. L. (2018). Cell-nonautonomous local and systemic responses to cell arrest enable long-bone catch-up growth in developing mice. *PLoS Biol* **16**, e2005086.

Rosello-Diez, A., Stephen, D. and Joyner, A. L. (2017). Altered paracrine signaling from the injured knee joint impairs postnatal long bone growth. *eLife* **6**.

Rowe, D. W., Adams, D. J., Hong, S. H., Zhang, C., Shin, D. G., Renata Rydzik, C., Chen, L., Wu, Z., Garland, G., Godfrey, D. A., et al. (2018). Screening Gene Knockout Mice for Variation in Bone Mass: Analysis by muCT and Histomorphometry. *Current osteoporosis reports* **16**, 77-94.

Šajn, L., Kononenko, I. and Milčinski, M. (2007). Computerized segmentation and diagnostics of whole-body bone scintigrams. *Computerized Medical Imaging and Graphics* **31**, 531-541.

Sanger, T. J., Norgard, E. A., Pletscher, L. S., Bevilacqua, M., Brooks, V. R., Sandell, L. J. and Cheverud, J. M. (2011). Developmental and genetic origins of murine long bone length variation. *Journal of experimental zoology. Part B, Molecular and developmental evolution* **316B**, 146-161.

Sears, K. E., Behringer, R. R., Rasweiler, J. J. t. and Niswander, L. A. (2006). Development of bat flight: morphologic and molecular evolution of bat wing digits. *Proc Natl Acad Sci U S A* **103**, 6581-6586.

Sheth, R., Marcon, L., Bastida, M. F., Junco, M., Quintana, L., Dahn, R., Kmita, M., Sharpe, J. and Ros, M. A. (2012). Hox genes regulate digit patterning by controlling the wavelength of a Turing-type mechanism. *Science* **338**, 1476-1480.

Shiratori, H., Yashiro, K., Shen, M. M. and Hamada, H. (2006). Conserved regulation and role of Pitx2 in situs-specific morphogenesis of visceral organs. *Development* **133**, 3015-3025.

Summerbell, D. (1977). Regulation of the deficiencies along the proximal distal axis of the chick wing-bud: a quantitative analysis. *J Embryol Exp Morphol* **41**, 137-159.

Taghizadeh, E., Terrier, A., Becce, F., Farron, A. and Büchler, P. (2019). Automated CT bone segmentation using statistical shape modelling and local template matching. *Computer Methods in Biomechanics and Biomedical Engineering* **22**, 1303-1310.

Weissheimer, A., Menezes, L. M., Sameshima, G. T., Enciso, R., Pham, J. and Grauer, D. (2012). Imaging software accuracy for 3-dimensional analysis of the upper airway. *Am J Orthod Dentofacial Orthop* **142**, 801-813.

Yiannakas, M. C., Mustafa, A. M., De Leener, B., Kearney, H., Tur, C., Altmann, D. R., De Angelis, F., Plantone, D., Ciccarelli, O., Miller, D. H., et al. (2016). Fully automated segmentation of the cervical cord from T1-weighted MRI using PropSeg: Application to multiple sclerosis. *NeuroImage: Clinical* **10**, 71-77.

Zhang, J., Yan, C. H., Chui, C. K. and Ong, S. H. (2010). Fast segmentation of bone in CT images using 3D adaptive thresholding. *Computers in Biology and Medicine* **40**, 231-236.